Supplementary Information for

Femtosecond Laser Direct Writing *Bombyx-mori*-sericin-based

Nanocomposites into Intrinsically Soft Wearable Micro/nano-

electronics

Qi Liang,[a] Qian Xu,[b] Gongwen Yang,[c] Yanting Xu,[c] Hanxuan Huang,[a] Zhishan Hou,[d] Zhengzhong Shao,[c] Ming Wang,[b] and Yun-Lu Sun*[a]

[a] School of Information Science and Technology, Fudan University, Shanghai 200433, China.

[b] Frontier Institute of Chip and System, Fudan University, Shanghai 200433, China.

[c] Department of Macromolecular Science, Fudan University, Shanghai 200433, China.

[d] International Science and Technology Cooperation Base for Laser Processing Robot, Zhejiang Provincial Key Laboratory of Laser Processing Robot, Wenzhou University, Wenzhou 325035, China.

*E-mail: ylsun@fudan.edu.cn

This file includes:

1, Supplement Figures

2, Supplement Tables

3, Supplement methods

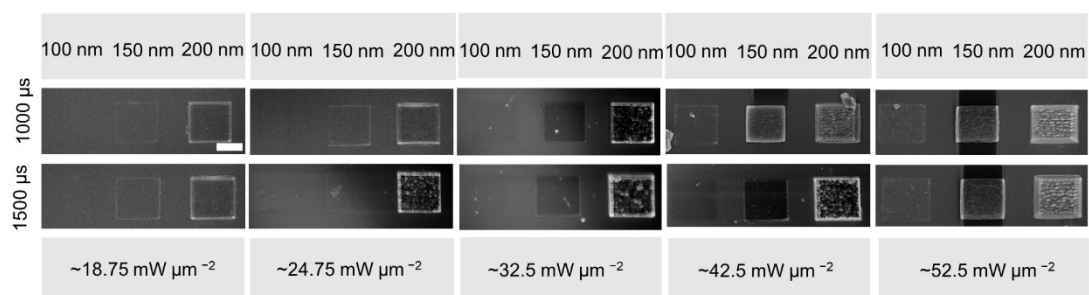**4, Supplementary Discussions**

1, Supplement Figures:

Figure S1. Optimization of FsLDW-processing parameters. Laser power intensity from about 18.75 to 52.5 mW μm^{-2}; scanning step from 100 nm to 200 nm; exposure time on single point, 1000 and 1500 μs, scale bar; 5 μm.
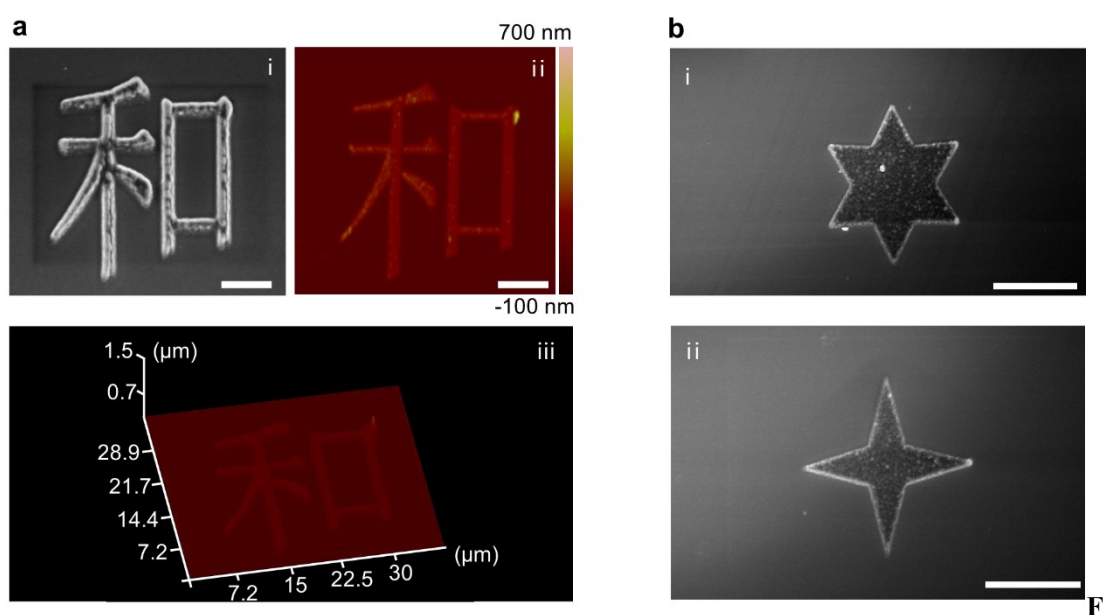

Figure S2. SEM and AFM images of sericin-based arbitrary geometric figures. **a**, sericin-based Chinese character '和'. (i) SEM image, (ii) 2D-view AFM image, (iii) 3D-view AFM image. **b,** (i) six-pointed star, (ii) four-pointed star; All above scale bars scale bar are 5μm.
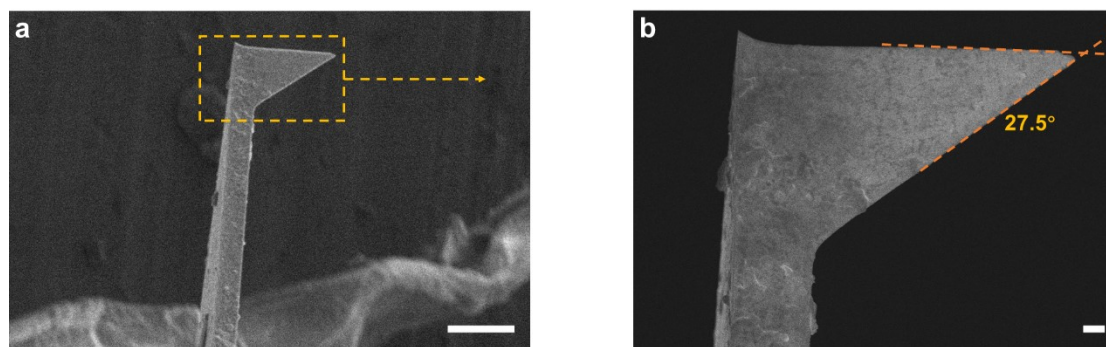
Figure S3. a, Parameters of the silicon nitride cantilever used for Young's modulus determination.

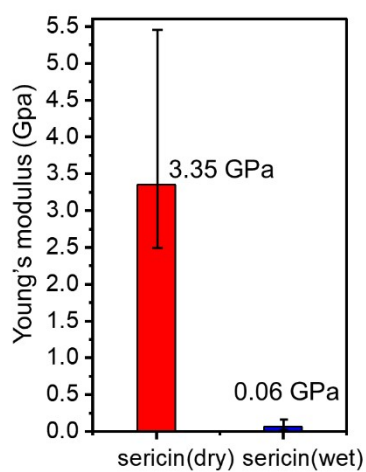**b,** SEM images of the silicon nitride cantilever; All above scale bars are 10 μm.

Figure S4. Comparison of the maximum Young's modulus of FsLDW-fabricated sericin-based

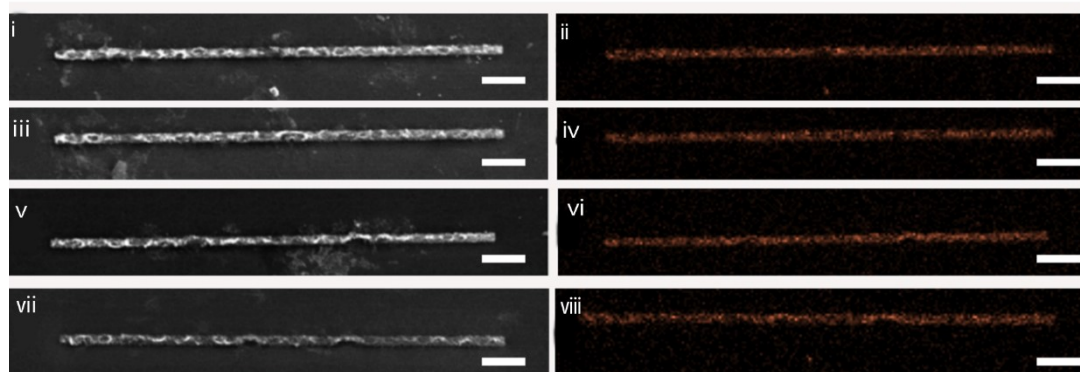biopolymers in various environments (air/water).

Figure S5. (i, iii, v, vii) SEM images of sericin/Ag nanocomposite microwires, (ii, iv, vi, viii) EDS

distribution maps of elemental Ag of sericin/Ag nanocomposite microwires, scale bars; 10 μm.

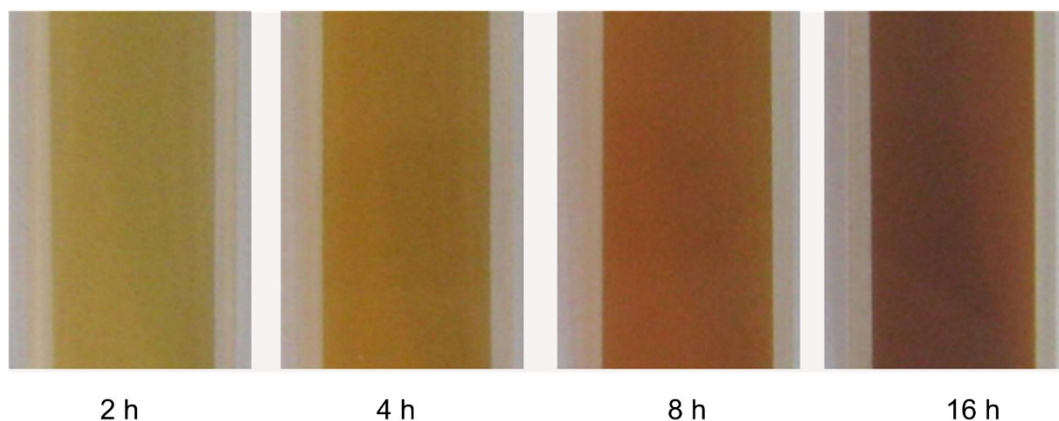**Figure S6.** Images of sericin/AgNO$_3$ aqueous resists pre-exposed for from 2 to 16 hours.
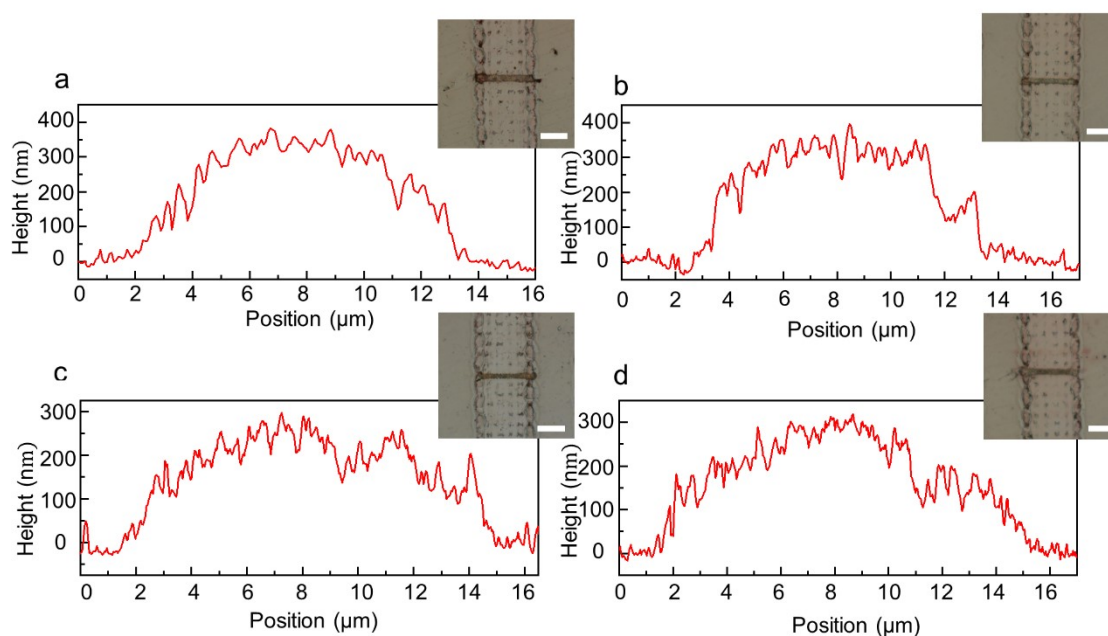

Figure S7. Cross-section profiles of sericin/Ag nanocomposite microwires fabricated by FsLDW from aqueous resists with 150 mg mL^{-1} sericin and different AgNO$_3$ concentrations. **a**, 25; **b**, 50; **c**, 75; **d**, 100; (unit, mg mL^{-1}), insets, optical microscopic (OM) images of sericin/Ag microwires, scale bars; 50 μm.
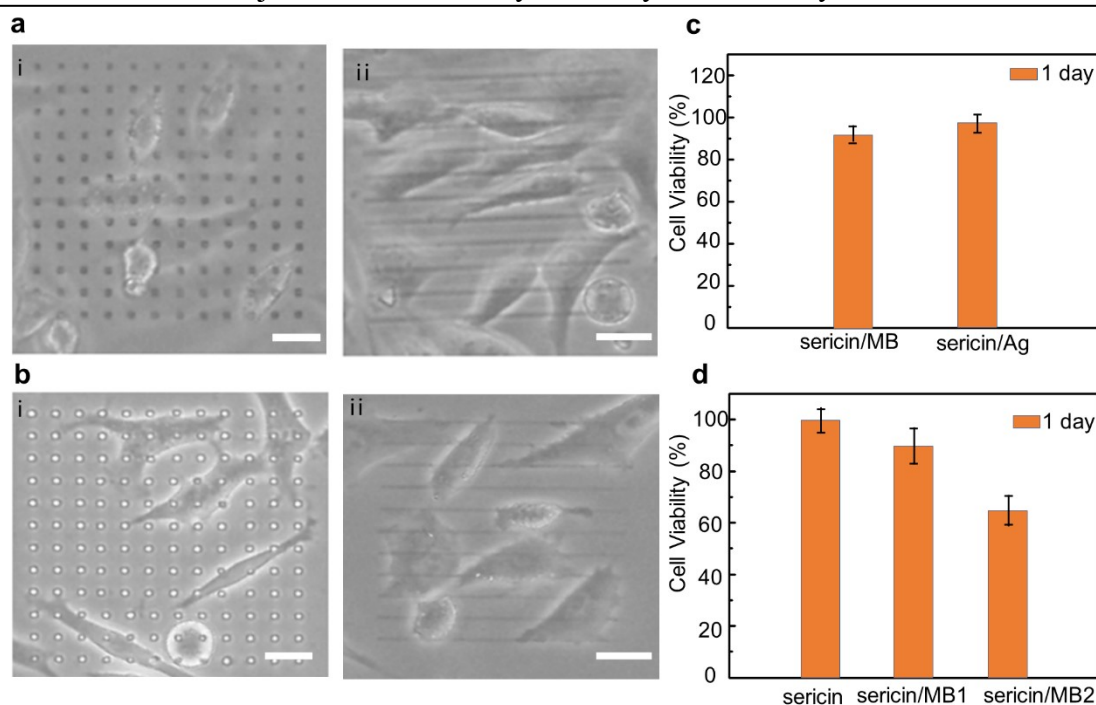
Figure S8. Cell culture based on FsLDW-fabricated sericin-based nanocomposite micro/nanostructures and aqueous resists. OM images of L929 cells cultured on the surface of two microstructures of **a**, pure sericin (i) microdot arrays (2×2 μm), (ii) microwire arrays (100×2 μm). **b**, sericin/Ag. (i) microdot arrays (2×2 μm), (ii) microwire arrays (100×2 μm). **c**, The survival rates of L929 cells after one day of culture on pure sericin and sericin/Ag nanocomposite microstructures. **d**, The survival rates of Hela cells after one day of culture on pure sericin, sericin/MB, and sericin/Ag aqueous resists. All above scale bars are10 μm.
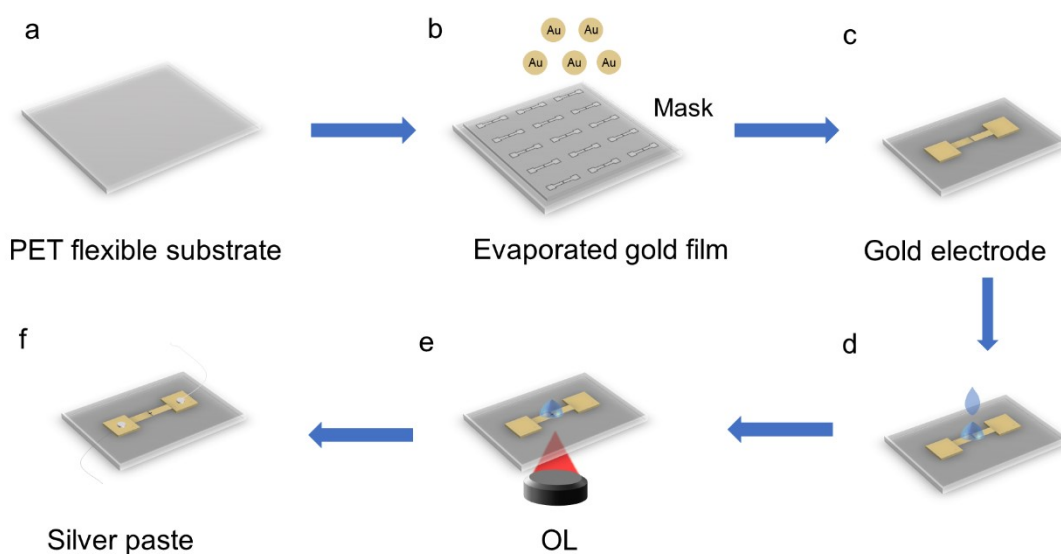
Figure S9. The preparation process of FsLDW-fabricated sericin/Ag nanocomposite microwires

flexible strain sensor.
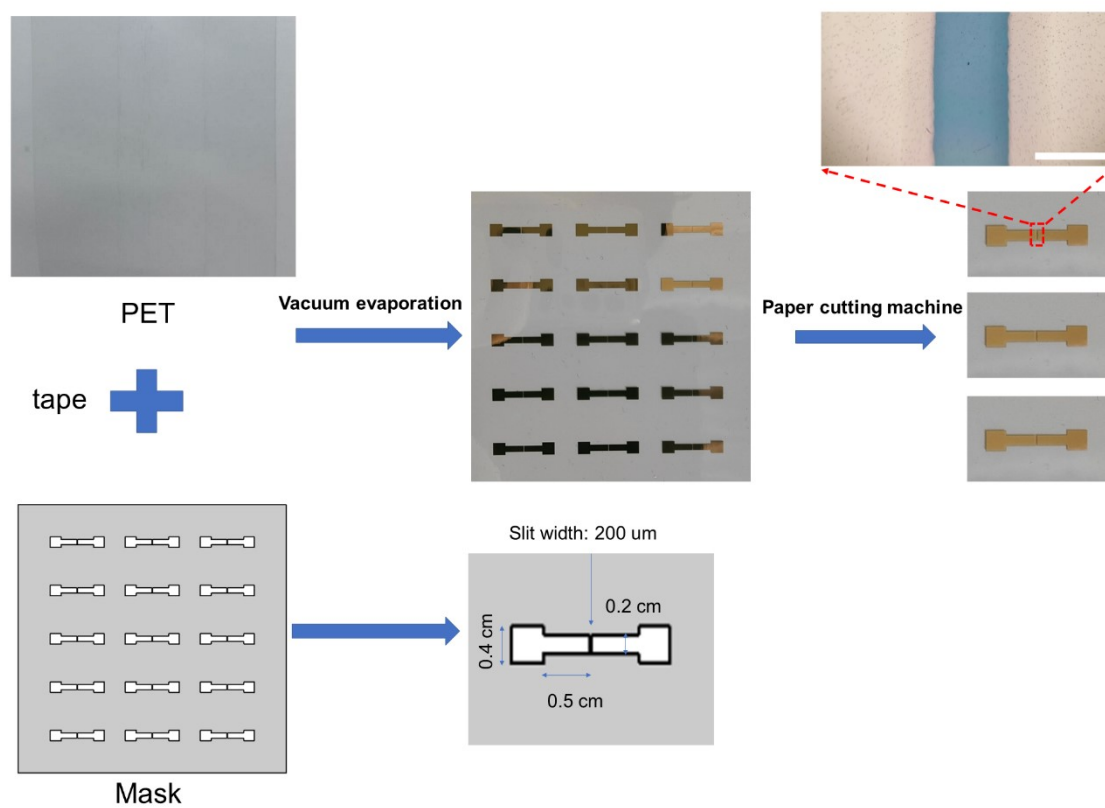
Figure S10. The detailed parameters of the mask, PET substrate and the separation process of and

the two gold electrodes, and the channel microscope image after evaporating the gold film.
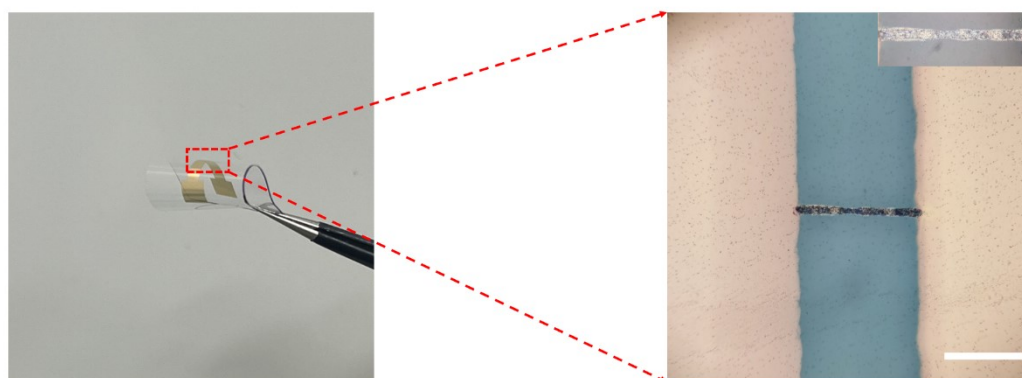
Figure S11. Schematic diagram of a bendable flexible strain sensor and its OM image.
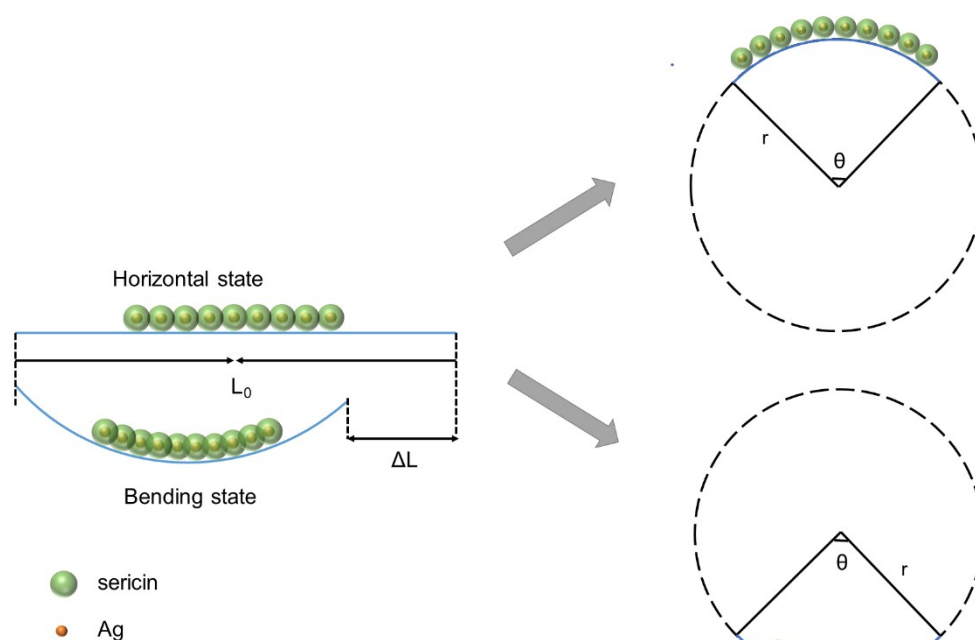
Figure S12. Schematic of the sensing mechanism of flexible strain sensors, the original length of the sensor (L_0) and the displacement of the outer measuring claw (ΔL), and bending radius of flexible strain sensor.
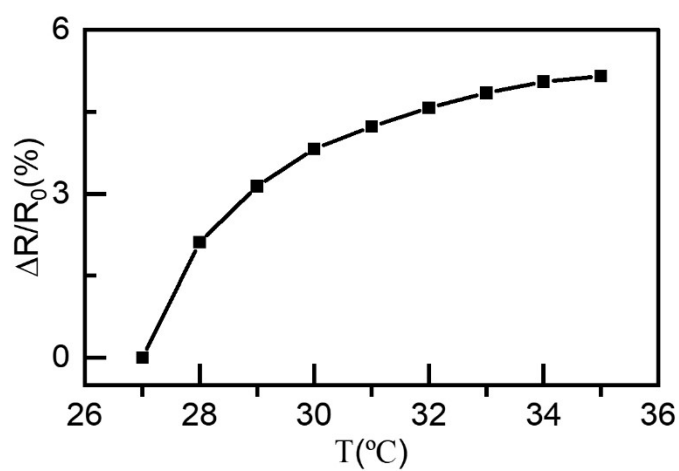
Figure S13. The relative resistance of the sensor with different temperatures.
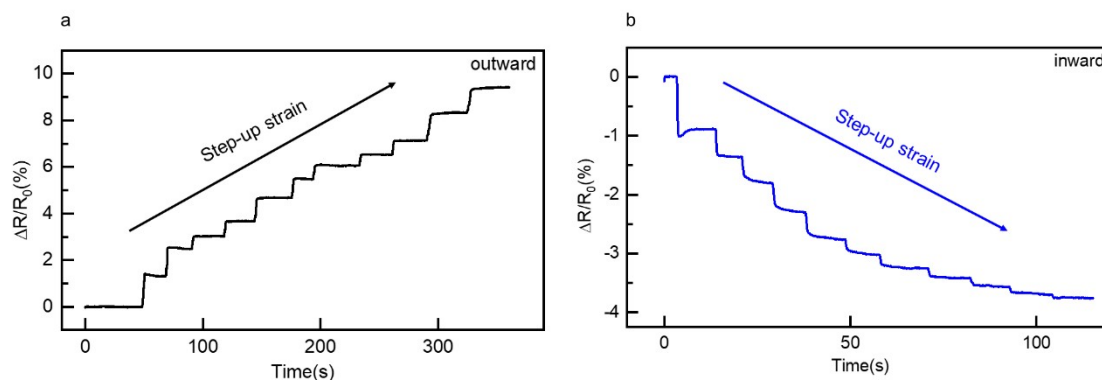
Figure S14. Changes in the relative resistance of strain sensors that are continuously bent. **a**, outwardly bending (0.15%~0.63%), and **b**, inwardly bending (-0.17%~-0.58%), respectively.
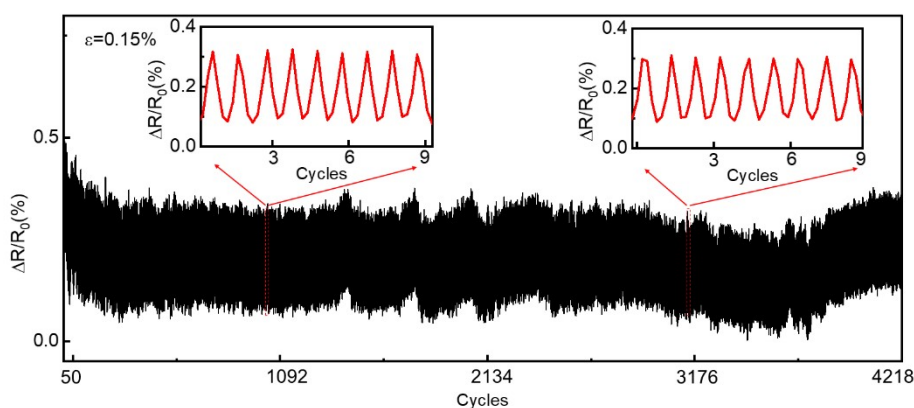
Figure S15. The flexible strain sensor is subjected to bending strains outward (ε=0.15%), and the bending and relaxation the relative resistance changes are repeated for ~4,200 cycles; insets show the relative resistance changes for 901-919 times and 3141-3149 times, respectively.
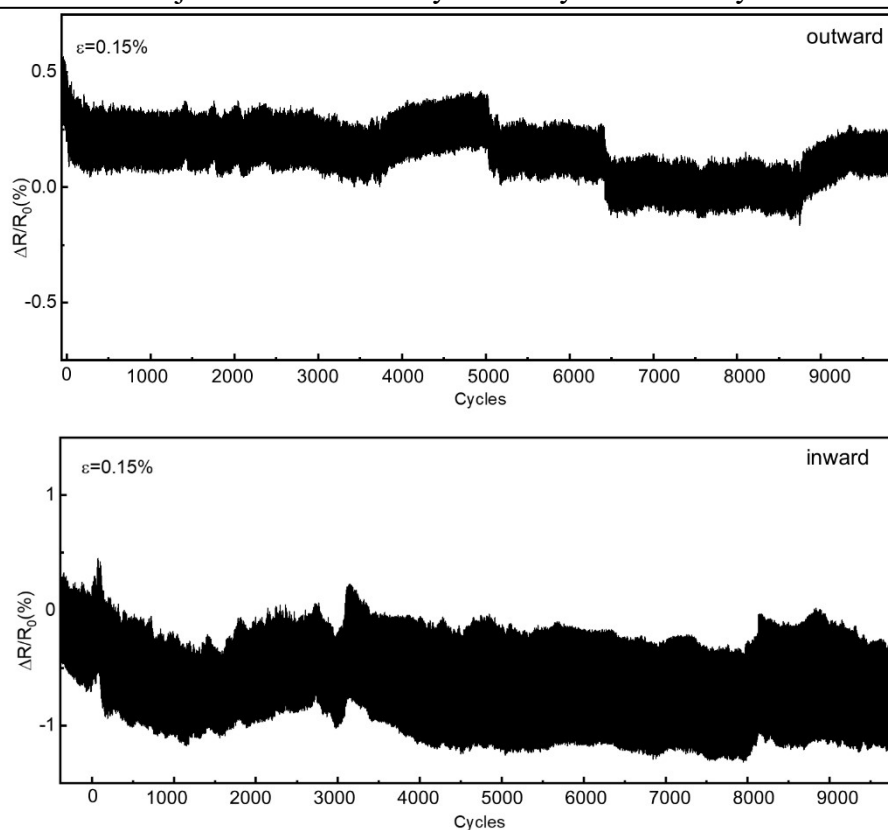
Figure S16. The flexible strain sensor is subjected to bending strains inward/outward ($\varepsilon=0.15\%$), and the bending and relaxation current changes are repeated for more than 10,000 cycles.
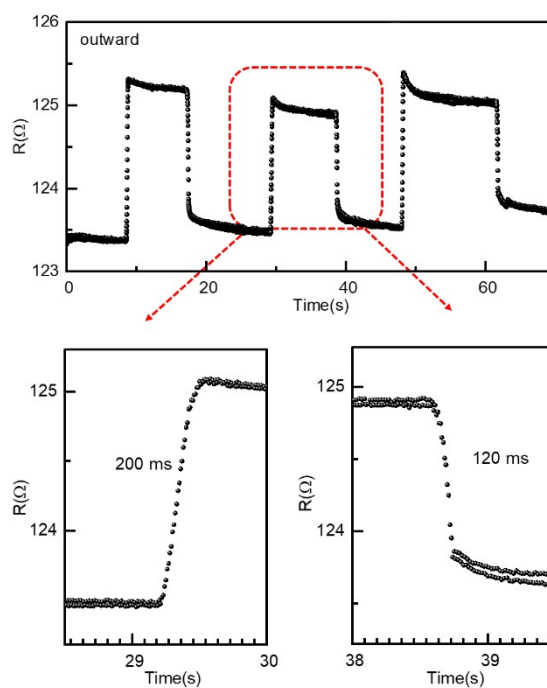
Figure S17. The response and recovery time of the strain sensor when an outward strain of 0.15% is applied.
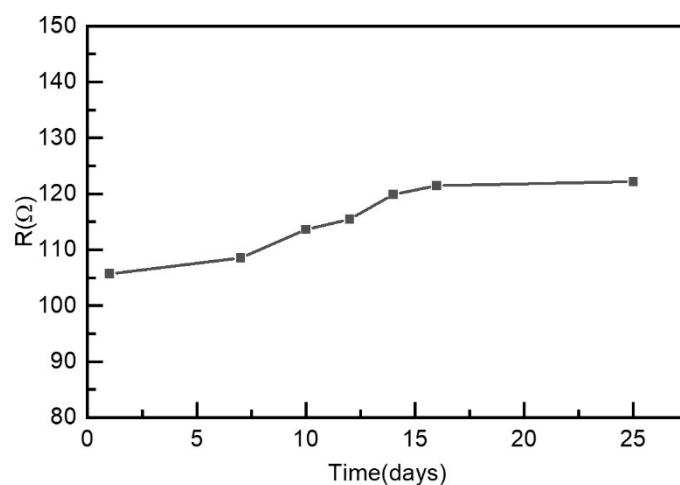
Figure S18. Stability of flexible strain sensors under atmospheric conditions. I-V curve of strain sensor under atmospheric conditions (0-25) days.
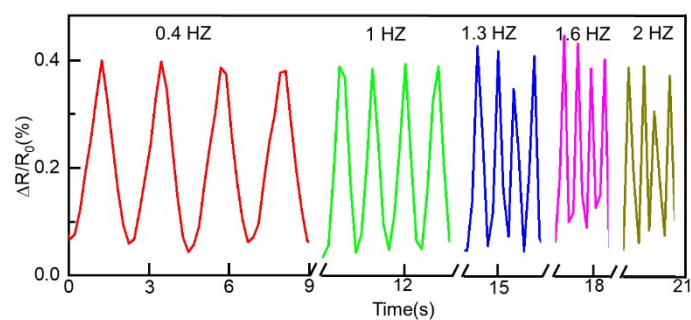
Figure S19. When outward bending strain is applied to the strain sensor for four consecutive cycles at frequencies of 0.4 Hz, 1 Hz, 1.3 Hz, 1.6 Hz, and 2 Hz, the relative resistance of the strain sensor changes.
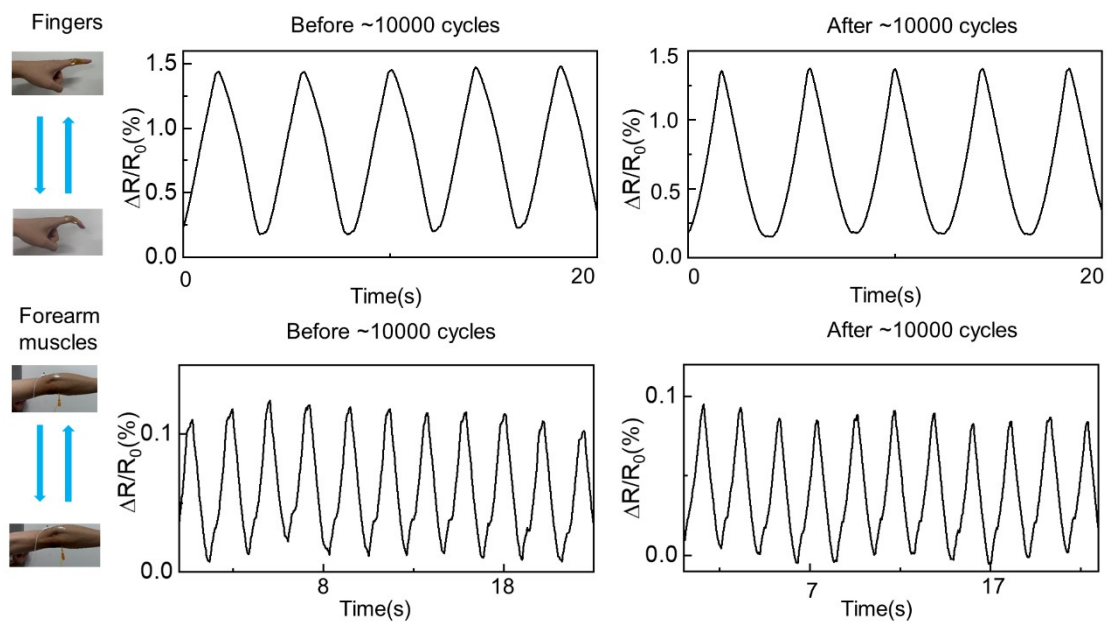
Figure S20. Changes in the relative resistance of the sensors to different body movements (e.g., fingers; forearm muscles) before and after long-term cycling (~10000 cycles).

2, Supplement Tables:

Supplementary Table S1. The parameters of the silicon nitride cantilever.

Lever					Tip	
Thickness (μm)	Length (μm)	Width (μm)	Spring const (N/m)	Resonant freq. (kHz)	Height (μm)	Radius (nm)
4.6	160	50	42	300	11	<10

Supplementary Table S2. The comparison of the electrical conductivity at room temperature (~26°C) between the microdevices fabricated in this work and some traditional metal materials.

Materials	Ag	Cu	Au	Zn	This work
Electrical conductivity (S m^{-1})	~6.30×10^7	~5.96×10^7	~4.52×10^7	~1.69×10^7	~1.68×10^5

Supplementary Table S3. Technical specification of equipment of the measurement setup.

Equipment	Technical specifications	
high-precision precision slide table	Resolution	0.02 mm
Keithley source meter	Voltage resolution	5 μV
	Current resolution	10 fA
	Temporal resolution	0.02 s
	Current limit	0.1 A

Supplementary Table S4. Technical specification of equipment of the measurement setup.

Materials	Gauge factor (GF)	Sensing scale	Ref
MXene-based hydrogel	60~80	0%-0.5%	[1]
(P:P@p-PSF) composite	6.25	1%-8%	[2]
AgNW/PDMS	2-14	0%-70%	[3]
AgNW/MoS2	5.96	0%-3%	[4]
CNTS/PU	14	0%-0.15%	[5]
Sericin/CNTs	-4	0%~15%	[6]
Sericin/Ag nanocomposites	16.95	0.15%~0.63%	This work

3, Supplement methods:

Extraction of silk sericin

According to the method for extracting silk sericin by Teramoto et al[7]., Fresh silk cocoons were taken and refined using the following method to obtain sericin protein with high purity. Clean cocoons (600 mg) were dissolved in LiBr solution (8 mol,24 mL), stirred, and dissolved at 35 °C for 24 h, then centrifuged at 3000 rpm for 15 min. The supernatant was mixed with Tris-HCl, the resulting solution pH~8, put into a dialysis bag with a molecular weight cut-off range of 6000-8000, and an appropriate amount of deionized water was for dialysis for 3 days. The water was changed in the middle 13 times, sericin solution with a concentration of about 1% was obtained, and the solution was dried and evaporated in a vacuum oven at 10 °C to obtain a powdered sericin solid.

Preparation of sericin-based aqueous resists for FsLDW

All aqueous resists in this work were prepared using ultrapure water (18.2 MΩ cm, 25 °C) from the MILLIPORE water purification system. Sericin/MB aqueous resists (~100 mg mL^{-1}, sericin~10 wt%, MB~0.18 wt%) were prepared by adding sericin (30 mg) to water (300 μL) followed by 0.6 mg of MB solid powder.

The sericin/AgNO$_3$ aqueous resists were prepared by blending sericin solution (300 mg mL^{-1}) and different AgNO$_3$ solutions as follows:

1, 1.5 mL sericin solution (300 mg mL^{-1}), 0.5 mLAgNO$_3$ solution (20 mg mL^{-1}, 100 mg mL^{-1}, 200 mg mL^{-1},300 mg mL^{-1}) = sericin~225 mg mL^{-1}, AgNO$_3$~5 mg mL^{-1}, 25 mg mL^{-1}, 50 mg mL^{-1}, 75 mg mL^{-1} (for EDS characterization)

2, 1.5 mL sericin solution (300 mg mL^{-1}), 0.5 mL AgNO$_3$ solution (8 mg mL^{-1}) = sericin~225 mg mL^{-1}, AgNO$_3$~2 mg mL^{-1} (sealed in a transparent centrifuge tube, 40 W incandescent 3 cm under the lamp for different time 0-24 h at 25 °C)

3, 1 mL sericin solution (300 mg mL^{-1}), 1 mL AgNO$_3$ solution (50 mg mL^{-1}, 100 mg mL^{-1}, 150 mg mL^{-1}, 200 mg mL^{-1},300 mg mL^{-1}) = sericin~150 mg mL^{-1}, AgNO$_3$~25 mg mL^{-1} ,50 mg mL^{-1}, 75 mg mL^{-1},100 mg mL^{-1}, 150 mg mL^{-1} (for sericin/Ag microfilament structure conductivity characterization)

4, 1 mL sericin solution (300 mg mL^{-1}) ,1 mL AgNO$_3$ solution (200 mg mL^{-1}) = sericin~150 mg mL^{-1}, AgNO$_3$~100 mg mL^{-1}(for preparation of micro flexible sensors)

FsLDW experimental procedures and parameters for different cases

For femtosecond laser parameters, the femtosecond laser (SpectraPhysics 3960-X1BB, 120 fs pulse width, 80 MHz repetition rate, 800 nm central wavelength) beam was tightly focused in sericin-based aqueous resists through a high numerical aperture Oil immersion objective lens (Olympus, numerical aperture = 1.35, ×60). The 3D scanning of the focused beam was realized based on the galvanometer (horizontal movements) and the piezo stage (Physik Instrumente P-622. ZCD, vertical movements). 3Ds Max designs arbitrary geometries of micro/nanostructures devices, corresponding computer-processed data were obtained, and FsLDW multiphoton lithography was realized by control software. After water rinsing, various complex micro/nanostructure devices could easily be fabricated on the substrate using FsLDW multiphoton lithography. During FsLDW-processing, excessively high laser intensity and prolonged processing times tended to induce overall or localized self-gelation of sericin solution. Meanwhile, considering the manufacturing quality and processing time, the process parameters of FsLDW were optimized. For all sericin/MB aqueous resists, the optimal FsLDW parameters were 42.5 mW μm^{-2} laser power intensity, 200 nm scan step size, and 1000 μs single point exposure time. For all sericin/AgNO$_3$ aqueous resists, the optimal FsLDW parameters were 22.5 mW μm^{-2} laser power intensity, 200 nm scan step size, and 1000 μs single point exposure time.

Determination of Young's Modulus Using the Hertzian Model

The indentation loading deflection–displacement curves in Fig 3ci were obtained using a Veeco MultiMode-8 AFM system (in air and water contact modes as needed) and Veeco's Silicon Nitride Cantilever (MLCT-AUNM)[8]. Data were analyzed using the Nanoscope-8.10 software. The silicon nitride cantilever's parameters are listed in Supplement Table S1. Based on the deflection-displacement curves, the Hertz model was used to simulate and calculate Young's modulus of sericin microstructures in dry air and immersed in water[9]. The formula is as follows:

$$E = \frac{2k\Delta d(1 - v^2)}{\pi(\Delta z - \Delta d)^2}tan\varphi$$

(1)

Where E is Young's modulus, Δd is the deflection of the probe cantilever, Δz is the displacement of the piezoelectric platform, k is the atomic force probe constant of 42 N m^{-1}, v is Poisson's ratio (v=0.5, φ is the angle of the probe tip, measured in the experiment is 27.5°, as shown in Supplement Fig. S3.

ITO/gold electrodes and conductivity testing

ITO electrode was purchased from South China Xiang Cheng Technology Co, Ltd. The film thickness is ~185 nm, and the resistance is ~6-8 ohms square^{-1}. Au electrode was prepared by thermal evaporation, with a film thickness of ~50 nm. The current-voltage curves of sericin/Ag nanocomposite microwires were measured using Keysight B1500A programmable voltage-current characterization system. During the test, the electrode bracket connected to the sample was fixed to avoid errors caused by electrode connection changes.

Calculation of conductivity

The calculation formula of conductivity (K) is as follows

$$K = \frac{GL}{S}$$

(2)

Where G is conductance (G=current/voltage), L is length, and S is cross-sectional area.

Fabrication of flexible strain sensor

The fabrication process of the strain sensor, which was made of sericin/Ag nanocomposite, is presented in Supplement Fig. S9. PET with good mechanical flexibility and high light transmission was used as a flexible substrate in this work, and the connecting parts were prepared. First, peeled off the protective film form the PET substrate to obtain a clean surface, and then used tape to adhere the mask to it. The bonding process ensured close contact between the formwork and substrate without gaps. Through vacuum thermal evaporation, two gold electrodes were deposited on a flexible PET substrate to form a ~200 μm channel. The detailed parameters of the template and the optical image of the channel separation between the two gold electrodes taken under the microscope are shown in Supplement Fig. S10. Then, used

a pipette to take sericin/AgNO$_3$ aqueous resists (sericin~150 mg mL^{-1}, AgNO$_3$~100 mg mL^{-1}, 10 μL), dropped it into the channel, adjusted the laser focus position, and prepared the sericin/Ag micro/nano-composite structure through FsLDW (laser parameter settings are as shown above). After FsLDW-fabrication processing, the uncross-linked portion was rinsed off with ultrapure water for 30 seconds and dried for 30 min. Finally, conductive silver glue (Beijing Xin Xing Bai Rui Technology Co. Ltd.) was used to connect silver wires to the gold electrodes on both sides to facilitate subsequent performance testing. The prepared flexible sensor and optical microscopy images of sericin/Ag nanocomposite are shown in Supplement Fig. S11.

Measurement

The measurement unit consists of a high-precision precision slide table and Keysight B1500A. The technical specifications of the equipment used in the measurement setup are listed in Supplement Table S3. A high-precision precision slide table was used to control the strain of the strain sensor; Keysight B1500A was used to test the strain sensor's performance, monitoring the sensor's current and resistance by applying a constant voltage of 0.1 V. During the detection process, the strain sensors attached to both ends of the outside of the high-precision precision sliding table are initially placed horizontally. One end of the strain sensor is fixed, and the sliding table controls the other. When in the horizontal position, the distance between the outer ends of the high-precision precision sliding table is the original length L$_0$ of the sensor, and the precise distance ΔL for sliding to achieve different movements is achieved (Supplement Fig. S12). The inner and outer surfaces of the strain sensor are bent respectively, and the geometric outline of the strain sensor is described as a circle with different bending radii. The original length L$_0$ is defined as

$$\frac{L_0}{2\pi r} = \frac{\theta}{360°}$$

(3)

The relationship between L_0 and θ can be calculated as

$$L_0 - \Delta L = 2r\sin\theta$$

(4)

Among them, r is the bending radius and θ is the central angle.

By combining (2) and (3), we can easily derive the equations for the moved bending distance and bending radius; the results are as follows

$$L_0 - \Delta L = 2r sin(\frac{L_0}{2r})$$

(5)

When the strain sensor is outwardly bent, the mechanical strain is calculated as $\varepsilon = \frac{2r}{h}$.

Similarly, the mechanical strain is calculated as $\varepsilon = \frac{-2r}{h}$ in the inward bending state, where h is the thickness of the PET substrate (50 μm)[10]. Apply a constant voltage (0.1 V) to the strain sensor. The resistance and current response were monitored, and the relative changes in the resistance of the strain sensor under different strain levels were calculated using the equation $((R-R_0)/R_0)$.

Other characteristics

OM images were acquired using a BA310Met metallographic microscope with a charge-coupled device. SEM characterization using field emission SEM (JSM-7500F, JEOL), AFM characterization of sericin-based micro/nanostructures morphology using Veeco NanoScope V in tapping mode in air. EDS analysis was performed using the AMETEK APOLO-XL EDS system integrated with the SEM system. Confocal microscopy characterization was performed with an Olympus FLUOVIEW-FV1000 confocal microscope.

Details of sericin-based FsLDW for cell culture

In this experiment, a mouse fibroblast cell line (L929) was cultured in Dulbecco's modified Eagle's medium (DMEM), and the medium was supplemented with 10% heat-inactivated fetal bovine serum (FBS) and antibiotics (100 μg mL^{-1} streptomycin and 100 μg mL^{-1} penicillin). All L929 cells were cultured in Cell Counting Kit (CCK-8) WST-8 in a humidified environment containing 5% CO_2 at 37°C. In the experiment, 2 -(2-methoxy-4-nitrophenyl)- 3 -(4-nitrophenyl)- 5 -(2,4-disulfophenyl)- 2H - (tetrazolium sodium glutamate) salt analysis was used to perform our cytotoxicity assessment assay. During the experiment, the 2D structure of pure sericin or sericin/Ag nanocomposite material prepared on the glass slide using FsLDW was used as the substrate for L929 cell attachment and culture. The entire glass sheet with 2D structure was sterilized by UV light irradiation for one hour. The sterilized glass slide was placed

into a 12-well cell culture plate. L929 cells were spread into cell culture plates, each well plate containing approximately 1.0×10^5 cells, and cultured for one day at 37°C and a 5% CO_2 atmosphere. To achieve good reproducibility, we performed three independent experiments, with three samples of independent L929 cell cultures simultaneously performed during each experiment. Then, the culture medium was replaced with serum-free fresh DMEM. At the same time, CCK-8 was placed in a dark environment as specified, and the cells were continued to be cultured for 2 hours. Finally, the entire sample was tested for absorbance at 450 nm using Exl 800 equipment (Biotek, USA).

Cell survival rate is calculated by the following formula:

$$Cell_v(\%) = \frac{([A]_t - [A]_b)}{([A]_c - [A]_b)} \times 100\%$$

(6)

Among them, $[A]_t$ represents the absorbance of the tested sample cells, $[A]_b$ represents the absorbance of the white plate sample without culture medium and cells, and $[A]_c$ represents the survival rate of cells without sericin protein micro-nanostructure.

During the experiment, we also immersed HeLa cells in a blended solution of pure sericin, sericin/MB, and sericin/AgNO$_3$ to test the toxicity of the solution. HeLa cells were seeded in a 96-well cell culture plate with culture medium (each well plate contained 1.0×10^4 cells) and cultured for 24 hours at 37°C in a 5% CO_2 atmosphere. Then, removed the medium and added 200 μL of DMEM. Solutions of MB with concentrations of 0.17 mg mL^{-1} and 0.34 mg mL^{-1} were added to DMEM, and then the cells were cultured for 1 hour. In order to ensure the reproducible effect of the experiment, three samples were prepared at the same time for each experiment, and the experiment was repeated three times. Then, the culture medium was replaced with serum-free fresh DMEM. At the same time, CCK-8 was placed in a dark environment as specified, and the cells were continued to be cultured for 2 hours. Finally, the entire sample was tested for absorbance at 450 nm using Exl 800 equipment (Biotek, USA). Calculate the cell survival rate according to the method above.

During the cell culture process, the pH of all cell culture solutions must be adjusted to neutral (~7.0). The osmotic pressure of the solution must also be adjusted to

approximately equal to the osmotic strength of 0.9 wt% NaCl aqueous solution; that is, the mass fraction 0.9% NaCl aqueous solution was used to prepare sericin, sericin/MB, sericin/AgNO$_3$ solution.

4, Supplementary Discussions

Supplementary Discussion 1

For probable mechanisms of sericin-centered FsLDW.

For sericin/MB inks, with the help of photosensitizer MB, covalent crosslinking of sericin occurred in the focal region. However, sericin molecules did not crosslink in pure sericin solutions, regardless of the femtosecond laser power density. The probable photochemical mechanisms of multiphoton crosslinking of sericin might be similar to previously reported multiphoton lithography of soluble and oxidizable proteins, such as cytochrome C, bovine serum albumin, lysozyme, and avidins[11–15]. Namely, the photosensitizer (MB) absorbs two photons under femtosecond laser irradiation with a central wavelength of 800 nm, generating $^1O_2$ or other oxidative substances, which in turn promotes crosslinking between sericin molecules. Accordingly, for sericin/AgNO$_3$ inks. Photoreduction of Ag$^+$ by 800 nm femtosecond laser is thought to occur by two-photon absorption induction[16–18]. Precious metal (Au, Ag, Pt, etc.) nanomaterials have been shown to act as photosensitisers to produce $^1O_2$ or other oxidising substances through two-photon absorption[19]. Moreover, metal nanoparticles have been shown to induce plasmonic resonance and enhance local electric fields under light radiation, greatly facilitating the reduction of additional metal ions in the surrounding environment, as well as the crosslinking and polymerization of cross-linkable (or polymeric) monomers[17]. The Ag nanoparticles generated during the FsLDW process acted as a photosensitizer. Therefore, under high-intensity femtosecond laser irradiation (FsLDW-processing parameters listed in Supplement Methods†), sericin crosslinking and Ag$^+$ photoreduction might co-occur[20,21].

Supplementary Discussion 2

For probable sensing mechanisms of sericin/Ag nanocomposite sensors.

Fig. S12 shows the sensing mechanism of sericin/Ag nanocomposite sensors. The sericin/Ag nanocomposite microwires were stretched when the outward strain was sensed. With the gradual increase of outward strain, sericin/Ag nanoparticles are gradually separated. The overlapping area between the Ag nanoparticles decreases and the spacing between the particles increases, thus hindering the tunnelling effect between the nanoparticles[22]. As a result, the resistance of the strain sensor gradually increases with the increase of outward strain. When inward strain was sensed, the opposite process occurred. When the sensor detected an inward strain, the sericin/Ag nanoparticle microwire was compressed. With the gradual increase of inward strain, the overlapping short chains of Ag nanoparticles are more tightly arranged and the particle spacing is reduced, which promotes the tunnelling effect between nanoparticles. Therefore, the resistance of the strain transducer decreased with increasing inward bending strain.

References

1   Zhang Y-Z, Lee KH, Anjum DH, Sougrat R, Jiang Q, Kim H *et al.* MXenes stretch hydrogel sensor performance to new limits. *Sci. Adv.* 2018; **4**: eaat0098.

2   Nie F, Gu Y-L, Zhao L, Li L-T, Shen F-X, Song J *et al.* Construction of conductive polymer coatings onto flexible PDMS foam composites with exceptional mechanical robustness for sensitive strain sensing applications. *Adv. Sensor Res.* 2024; **3**: 2300140.

3   Amjadi M, Pichitpajongkit A, Lee S, Ryu S, Park I. Highly stretchable and sensitive strain sensor based on silver nanowire–elastomer nanocomposite. *ACS Nano* 2014; **5**: 5154-5163.

4   Lan L, Yin T, Jiang C, Li X, Yao Y, Wang Z *et al.* Highly conductive 1D-2D composite film for skin-mountable strain sensor and stretchable triboelectric nanogenerator. *Nano Energy* 2019; **62**: 319–328.

5   Gao Y, Guo F, Cao P, Liu J, Li D, Wu J *et al.* Winding-locked carbon nanotubes/polymer nanofibers helical yarn for ultrastretchable conductor and strain sensor. *ACS Nano* 2020; **14**: 3442–3450.

6   Duan Q, Lu Y. Silk sericin as a green adhesive to fabricate a textile strain sensor with excellent electromagnetic shielding performance. *ACS Appl Mater Interfaces* 2021; **13**: 28832–28842.

7   Teramoto H, Miyazawa M. Molecular orientation behavior of silk sericin film as revealed by ATR infrared spectroscopy. *Biomacromolecules* 2005; **6**: 2049–2057.

8   Efremov YM, Okajima T, Raman A. Measuring viscoelasticity of soft biological samples using atomic force microscopy. *Soft Matter* 2019; **16**: 64–81.

9   Cundall PA. Computer simulations of dense sphere assemblies. *Stud. Appl. Mech.* 1988; **20**: 113–123.

10   Zhang Z, Si T. Controllable assembly of silver nanoparticles based on the coffee-ring effect for high-sensitivity flexible strain gauges. *Sens. Actuator A Phys.* 2017; **264**: 188–194.

11   Dawood F, Qin S, Li L, Lin EY, Fourkas JT. Simultaneous microscale optical manipulation, fabrication and immobilisation in aqueous media. *Chem. Sci.* 2012; **3**: 2449–2456.

12   Connell JL, Ritschdorff ET, Whiteley M, Shear JB. 3D printing of microscopic bacterial communities. *PNAS* 2013; **110**: 18380–18385.

13   Khripin CY, Brinker CJ, Kaehr B. Mechanically tunable multiphoton fabricated protein hydrogels investigated using atomic force microscopy. *Soft Matter* 2010; **6**: 2842–2848.

14   Spivey EC, Ritschdorff ET, Connell JL, McLennon CA, Schmidt CE, Shear JB. multiphoton lithography of unconstrained Three-Dimensional protein microstructures. *Adv. Funct. Mater.* 2013; **23**: 333–339.

15   Pitts JD, Howell AR, Taboada R, Banerjee I, Wang J, Goodman SL *et al.* New photoactivators for multiphoton excited three-dimensional submicron cross-linking of proteins: bovine serum albumin and type 1 collagen. *Photochem. Photobiol.* 2002; **76**: 135–144.

16   Tanaka T, Ishikawa A, Kawata S. Two-photon-induced reduction of metal ions for fabricating three-dimensional electrically conductive metallic microstructure. *Appl. Phys. Lett.* 2006; **88**: 081107

17   Xu B-B, Wang L, Ma Z-C, Zhang R, Chen Q-D, Lv C *et al.* Surface-plasmon-mediated programmable optical nanofabrication of an oriented silver nanoplate. *ACS Nano* 2014; **8**: 6682–6692.

18   Shukla S, Vidal X, Furlani EP, Swihart MT, Kim K-T, Yoon Y-K *et al.* Subwavelength direct laser patterning of conductive gold nanostructures by simultaneous photopolymerization and photoreduction. *ACS Nano* 2011; **5**: 1947–1957.

19   Jiang C, Zhao T, Yuan P, Gao N, Pan Y, Guan Z, Zhou N, Xu Q-H, Two-photon induced photoluminescence and singlet oxygen generation from aggregated gold nanoparticles. *ACS Appl. Mater. interfaces* 2013; **5**: 4972-4977

20   Shukla S, Furlani EP, Vidal X, Swihart MT, Prasad PN. Two-photon lithography of sub-wavelength metallic structures in a polymer matrix. *Adv. Mater.* 2010; **22**: 3695–3699.

21   Ma Z-C, Zhang Y-L, Han B, Chen Q-D, Sun H-B. Femtosecond-laser direct writing of metallic micro/nanostructures: from fabrication strategies to future applications. *Small Methods* 2018; **2**: 1700413.

22   Amjadi M, Kyung K-U, Park I, Sitti M. Stretchable, skin-mountable, and wearable strain sensors and their potential applications: a review. *Adv. Funct. Mater.* 2016; **26**: 1678–1698.